

JGR Atmospheres

RESEARCH ARTICLE

10.1029/2019JD031191

Key Points:

- A best combination of WRF physical schemes for tropical weather simulations is proposed through sensitivity study
- Applying cool coating on all urban surfaces in Singapore provides a nocturnal UHI mitigation efficiency of 30–38% in residential areas
- Cool roofs provide more urban cooling effect than walls and roads. Cool coating effect is more significant in low anthropogenic heat areas

Supporting Information:

- Supporting Information S1

Correspondence to:

W. M. Pun,
mpwan@ntu.edu.sg

Citation:

Zhou, M., Long, Y., Zhang, X., Donthu, E. V. S. K. K., Ng, B. F., & Wan, M. P. (2020). Sensitivity Study of Weather Research and Forecasting Physical Schemes and Evaluation of Cool Coating Effects in Singapore by Weather Research and Forecasting Coupled with Urban Canopy Model Simulations. *Journal of Geophysical Research: Atmospheres*, 125, e2019JD031191. <https://doi.org/10.1029/2019JD031191>

Received 18 JUN 2019

Accepted 9 MAY 2020

Accepted article online 16 MAY 2020

Corrected 21 APR 2021

This article was corrected on 21 APR 2021. See the end of the full text for details.

Author Contributions:

Conceptualization: Mandi Zhou
Data curation: Mandi Zhou
Formal analysis: Mandi Zhou, Yongping Long
Investigation: Mandi Zhou, Yongping Long
Methodology: Mandi Zhou
Resources: Mandi Zhou
Software: Mandi Zhou
Supervision: Mandi Zhou
(continued)

©2020. American Geophysical Union.
All Rights Reserved.

Sensitivity Study of Weather Research and Forecasting Physical Schemes and Evaluation of Cool Coating Effects in Singapore by Weather Research and Forecasting Coupled with Urban Canopy Model Simulations

Mandi Zhou¹, Yongping Long^{2,3}, Xiaoqin Zhang¹, Eswara V. S. K. K. Donthu¹, Bing Feng Ng³ , and Man Pun Wan³ 

¹Energy Research Institute, Nanyang Technological University, Singapore, ²Energy Research Institute, Interdisciplinary Graduate Programme, Nanyang Technological University, Singapore, ³School of Mechanical and Aerospace Engineering, Nanyang Technological University, Singapore

Abstract Mesoscale meteorological modeling was conducted to evaluate air temperature at 2-m above surface (T2), wind speed/direction, and relative humidity (RH) in Singapore, a tropical city, for a dry period. A sensitivity study was conducted to determine the best combination of schemes for the physical modules. The model was used to study the urban heat island (UHI) effect and urban cooling effect by applying cool coating on various urban surfaces. Maximum UHI intensity of 3.2°C is found at nighttime (21:00) at a hot spot in the Commercial/Industrial area. At nighttime, when the UHI effect is generally more intense than daytime, applying cool coating on all urban surfaces can reduce the UHI effect by about 30% in residential areas and about 6% in commercial/industrial areas. Maximum T2 reduction of 3.1°C and surface skin temperature (TSK) reduction of 9.8°C due to cool coating is found at 13:00 at certain locations. The cool urban surfaces reduce radiative heat absorption during daytime, reducing heat storage in urban structures. This leads to subsequent reduction of stored heat release from urban structures, mitigating UHI effect during nighttime. Applying cool coating on horizontal surfaces (roofs and roads) provides more cooling effect than vertical surfaces (walls). Cool roofs provide more cooling effect than cool roads since roofs cover more urban horizontal surfaces than roads do in the current setting. Part of the radiation reflected by cool roads could be absorbed by other urban structures, reducing its cooling effect as compared to cool roofs.

1. Introduction

Many studies have shown that the urban heat island (UHI) effect exacerbates heat-related health risks to urban population (Heaviside et al., 2017; Kovats & Hajat, 2008; Yow, 2007), whereby ambient temperatures in urban areas are often observed to be higher than those in surrounding less-urbanized areas, particularly at night. UHI effect is mainly caused by the modification of land surfaces due to urban development, for example, replacing natural surfaces by paving or construction of buildings. Typical materials (such as concrete, tarmac, and asphalt) used to construct urban structures generally absorb, retain, and, subsequently, re-radiate more heat than natural surfaces. Natural cooling effect due to evaporation from natural surfaces and evapotranspiration from vegetation is also removed by urban developments. High density of building structures hinders natural ventilation by wind. Additionally, high concentration of human activities in cities leads to high anthropogenic heat flux (Oke, 1982). UHI could cause health- and environment-related issues. Hot weather has been associated with heat exhaustion, heatstroke, emergency hospitalizations, and death (Hajat et al., 2014; Heaviside et al., 2017, 2018). Raised urban temperature also leads to increased energy consumption by air-conditioning systems, especially in cities located in warm climate regions, which could subsequently lead to raised pollution emission due to energy generation (Li & Zhao, 2012). Mitigating the UHI effect could potentially reduce energy consumption, emissions of air pollutants and greenhouse gases in urban areas, and heat-related risks to human health and well-being (United States Environmental Protection Agency, 2008).

Various UHI effect mitigation strategies are studied and adopted in an effort to reduce urban heat (Kardinal Jusuf et al., 2007). In particular, materials used in the urban fabrics play a very important role in urban

Validation: Mandi Zhou
Visualization: Mandi Zhou
Writing - original draft: Mandi Zhou,
Yongping Long
Writing - review & editing: Mandi
Zhou, Yongping Long, Xiaoqin Zhang,
Eswara V. S. K. K. Donthu, Bing Feng
Ng

thermal balance as they absorb incident solar radiation and dissipate part of the absorbed heat through convective and radiative processes to the urban atmosphere (Mohajerani et al., 2017). Mitigation strategies such as albedo modification, cool or vegetated roofs, or urban vegetation and greenspace have been proposed (Chen et al., 2011). In particular, applying solar reflective (high albedo) cool coating on the surfaces of urban structures could effectively cool down the surrounding air by reducing the absorption of solar radiation by urban structures (Synnefa et al., 2008).

The Weather Research and Forecasting (WRF) model (National Center for Atmospheric Research, USA 2008) coupled with urban parameterization schemes (Kusaka et al., 2001) has been widely used for urban mesoscale simulations in many studies, including the evaluation of performance of various UHI effect mitigation strategies on local conditions (Chen et al., 2011). Georgescu et al. (2014) employed WRF with four-layer Noah land surface model to predict the warming of the United States in Year 2100. They suggested that full deployment of cool roofs can reduce 1.47°C in California. Macintyre et al. (2017) and Macintyre and Heaviside (2019) employed WRF coupled with building energy parameterization (BEP) modeling to reveal the effects of heatwave and UHI on the environment and society. They suggested that using cool roofs to reduce local ambient temperatures is an effective solution to health risks caused by excessive urban heat. They suggested that cool roofs could reduce city center daytime T2 by 0.5°C on average, and up to a maximum of 3°C, leading to ~23% reduction of average UHI intensity and ~25% reduction of heat-related mortality during a heatwave. Liu et al. (2018) employed the WRF-Urban Canopy Model (UCM) to evaluate the strategies of applying cool roofs and green roofs for western China. Their study revealed that cool roofs reduced urban T2 by about 0.51°C due to enhanced reflection of solar radiation whereas green roofs reduced urban T2 by about 0.39°C due to additional evaporation/evapotranspiration. Morini et al. (2016) employed WRF-UCM to study the effect of increasing albedo of roofs on the UHI effect in Terni, Italy. They indicated that increasing roof albedo could effectively decrease the UHI effect during both daytime and nighttime by 2°C.

Singapore is a highly urbanized (100% urbanization) city-state located in the tropical area (between 1°09'N to 1°29'N, and 103°36'E to 104°25'E) (Central Intelligence Agency, 2018). UHI effect is found to be significant in Singapore, reaching 7.1°C in May 2003, by in situ measurements (Quah & Roth, 2012). Singapore is subjected to wet equatorial climate with negligible seasonal variation (mean monthly air temperature varies between roughly 26–28°C and small diurnal variation in air temperature (mean daily minimum air temperature ranges from about 24–26°C and daily maximum air temperature ranges from about 30–33°C) (Meteorological Service Singapore, 2018). The annual incoming solar radiation can reach about 1,600 kWh/m² (Energy Market Authority, 2016), much higher than the global average of 1,120 kWh/m² (Newport Corporation, 2019). The annual rainfall total exceeds 2,000 mm (Meteorological Service Singapore, 2018). Applying cool coatings on the surfaces of urban structures could be a way to mitigate the UHI effect in Singapore. Li et al. (2013) and Li and Norford (2016) employed WRF-UCM model to evaluate the mitigation effect of the cool roofs in Singapore. They revealed that cool roofs could reduce the T2 and TSK by up to 1.4°C and 5.5°C during daytime.

Despite the fact that mesoscale effectiveness of cool roofs on mitigating UHI was investigated in several cities in different climate regions, the effectiveness of applying cool coatings on different urban surfaces, for example, building walls and roads, which account for large portions of urban surfaces in highly developed cities, has received less attention. In this work, WRF-UCM model is adopted to evaluate cool coating as an UHI mitigation strategy in Singapore. A sensitivity study was conducted to determine the best combination of schemes for major physical modules when setting up the WRF model to ensure its robustness. The effects of applying cool coating on different types of urban surfaces on urban cooling are simulated. Mesoscale impact of cool coatings applied on roofs, walls, and roads are investigated individually and in combinations. The effect of cool coating on urban heat balance is analyzed. This work provides a platform for the evaluation of UHI mitigation strategies using solar reflective materials in Singapore and provides support to strategies that employ cool coating for urban heat reduction.

2. Methodology

2.1. Area of Interest

The area of interest covers all land territories of Singapore together with some land territories of Southern Malaysia (part of the Johor area) and Indonesia (part of the Riau Islands area) as well as the sea surface

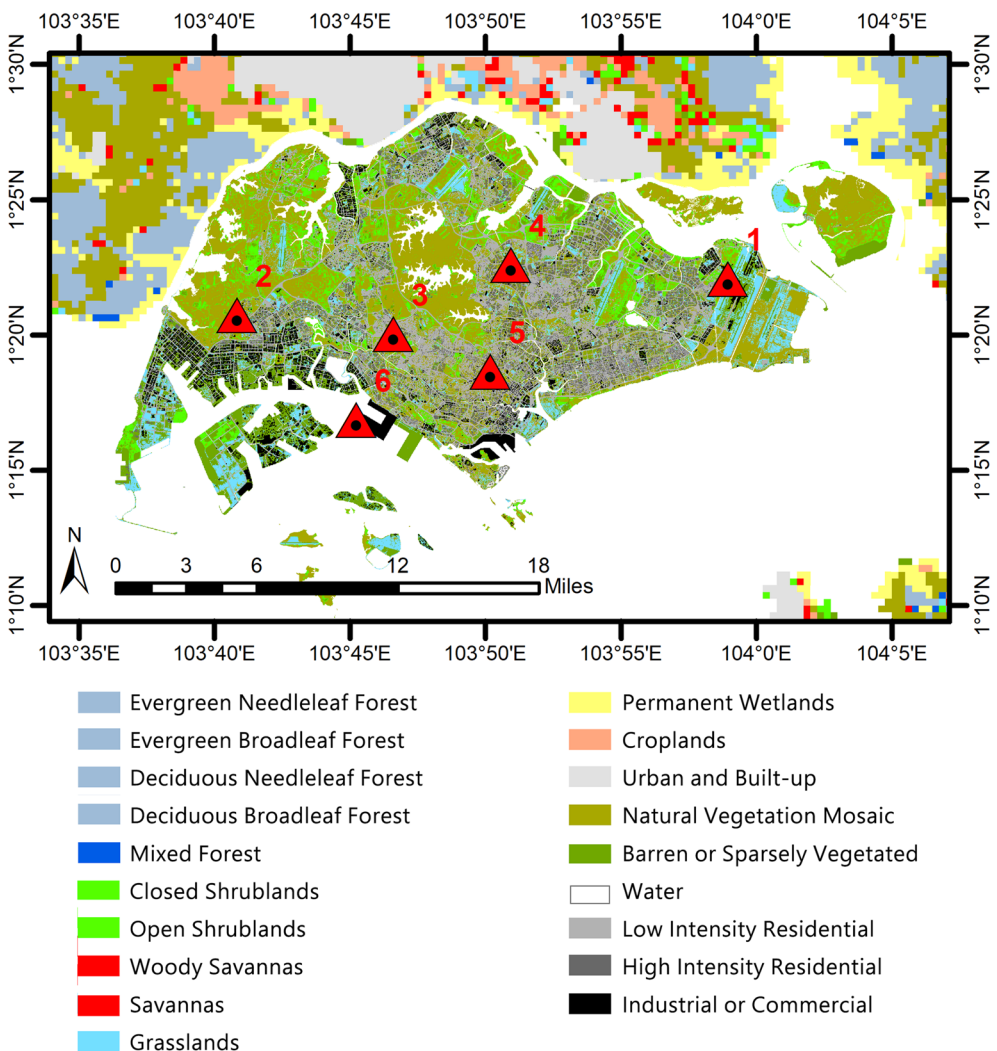


Figure 1. Land use/land cover map and the locations of the six selected weather stations in Singapore.

in between these regions, as shown in Figure 1. For Singapore land territories, high-resolution land use/land cover (LULC) data obtained from 2.5-m horizontal resolution Cartosat 1 (Satellite Imaging Corporation, 2016) and 12-m vertical resolution Digital Surface Model from Tandem X (EOportal, 2014) at 2-m accuracy are used together with the Singapore Master Plan 2014 (MP14) (Urban Redevelopment Authority Singapore, 2014). The spatial resolution of the land use map is 10 m × 10 m per pixel.

All urban land use areas in Singapore land territories defined in the abovementioned data set were categorized into residential and commercial/industrial (C/I) land use categories with reference to MP14. The residential category is further divided into low-intensity residential (LIR) and high-intensity residential (HIR) categories according to the vegetation fraction in each pixel retrieved from Cartosat 1 data. For residential areas, pixels with 20–70% vegetation fraction are categorized as LIR and those with less than 20% vegetation fraction are categorized as HIR. Pixels having vegetation fractions above 70% are excluded from urban categories but are assigned into six International Geosphere–Biosphere Programme (IGBP) classes, that is, Water, Evergreen Broadleaf Forest, Permanent Wetlands, Open Shrublands, Grasslands, and Barren or Sparsely Vegetated, by unsupervised Iterative Self-Organizing Data Analysis Technique Algorithm (ISODATA) clustering (Oak Ridge National Laboratory Distributed Active Archive Central, 2016). HIR, LIR, and C/I account for 6.03%, 7.40%, and 7.74%, respectively, of Singapore land surface area in the land use map. The pixels in the 10-m resolution land use map were then aggregated to 90-m resolution by combining 9 × 9 10-m pixels to one 90-m pixel (90 m × 90 m). Urban fraction in each 90-m pixel was determined

Table 1
Measurement Data of Weather Stations Used in the Sensitivity Study

No.	Location	District	Lat. (N)	Long. (E)	Area use
1	Changi Airport	Changi	1.37	103.98	Airport
2	Nanyang Technological University	Jurong (West)	1.35	103.68	Educational
3	Ngee Ann Polytechnic	Clementi	1.33	103.78	Educational
4	Ang Mo Kio Avenue 8	Ang Mo Kio	1.38	103.85	Residential
5	Scotts Road	Newton	1.31	103.84	Commercial
6	Pasir Panjang Terminal	Pasir Panjang	1.28	103.75	Sea port

by dividing the total number of urban 10-m pixels found in each 90-m pixel by 81 (9×9). The urban category that contributes the largest number of 10-m pixels in each 90-m pixel becomes the urban category of that 90-m pixel. A 90-m pixel will become a nonurban pixel if there is no urban 10-m pixel inside. Its category was defined following the category that contributes the largest number of 10-m pixels in it. This processing method creates a land use/land cover map and an urban fraction map, which allows each urban pixel (90-m) to have individual urban fraction, for importing to WRF-UCM.

Based on the Digital Surface Model (EOportal, 2014) data, the average building height and average roof width in each urban pixel (LIR, HIR, and C/I, 90-m) were obtained. Average road width per pixel was determined by overlaying the road data layer based on MP14 onto the LULC

map. Averages of building heights, roof, and road widths of all pixels in each urban category were then be taken for subsequent modeling input in UCM. The ArcGIS Geoprocessing tools and an in-house developed Python scripts were used to perform the above operations.

For regions outside of Singapore land territories, the map data were generated using 15' MODIS 20-category LULC data (Oak Ridge National Laboratory Distributed Active Archive Central, 2016). In these regions, all urban land use areas were categorized into a “Urban and Built-up” category, which accounted for 6.13% of surface (land and sea) area in the area of interest. These “Urban and Build-up” areas were subsequently recognized as HIR in UCM, and the urban fraction was generated using the National Urban Data and Access Portal Tool (NUDAPT) data set (Ching et al., 2009).

Observation data from six selected weather stations in Singapore, as indicated in Figure 1, was used for comparison with WRF-UCM simulation results in this study. Locations of these six selected stations are summarized in Table 1.

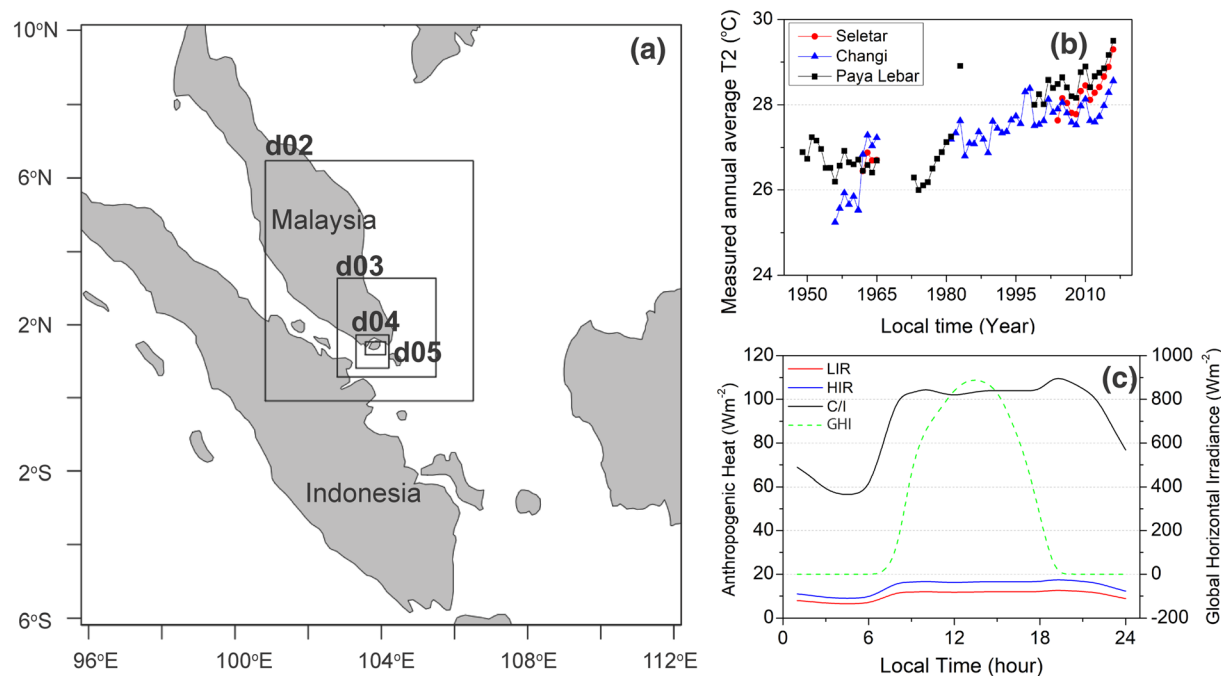


Figure 2. (a) The five nested domains used in WRF-UCM modeling; (b) Annual mean T2 from Weather Station Records; (c) AH profiles of urban land use categories and averaged GHI from 2 to 7 July 2016.

Table 2
General WRF Model Configuration

Geographical input data	High-resolution land use data
Grid spaces of five domains	24.3 km, 8.1 km, 2.7 km, 0.9 km, 0.3 km
Vertical layers	32 layers
Meteorological input	NCEP GDAS/FNL 0.25 Degree Global Tropospheric Analyses and Forecast Grids
Start time	01/07/16–0:00 UTC (Coordinated Universal Time), UTC = LT – 8 for Singapore
End time	08/07/16–0:00 UTC
Shadow module	On
Land surface model	Noah land surface model (LSM)
Output frequency	Hourly

data sets from NCAR (The Data Engineering and Curation Section of the Computational and Information Systems Laboratory at the National Center for Atmospheric Research in Boulder, Colorado, 2015).

The WRF-UCM simulation period is from 1 to 7 July 2016. The first 24 hr of the simulation period was used for model spin-up; that is, the simulation results of this 24 hr would be disregarded in subsequent analysis. From observation data, 2016 was the hottest year in Singapore in the past 7 decades till this study. The highest average annual air temperature at 2-m height (T2) was recorded in this year based on the measurements in three weather stations that have long-term observation data in Singapore, as shown in Figure 2b. The selected period in July for simulation had the longest period of consecutive dry days in 2016. This period was selected because high UHI intensity in Singapore happens during periods of consecutive dry days when urban structures are subjected to a sustained period of diurnal solar radiation cycles without experiencing the cooling effects from rainfall (Meteorological Service Singapore, 2012; Roth & Chow, 2012). This period was also used for the subsequent simulation study of the effects of cool coating on UHI mitigation. Cumulus module was turned off in the inner three domains since they are smaller than the minimum spatial resolution (3 km) of the module (University Corporation for Atmospheric Research, Boulder, CO, 2012). Details of model configuration are shown in Table 2.

Anthropogenic heat (AH) and its diurnal variation profiles for Singapore (Quah & Roth, 2012), as shown in Figure 2c, were input into the UCM as a part of the sensible heat flux from the urban canopy layer. AH information reported in Quah and Roth (2012) was derived based on data available for 2008 and 2009, meaning

that this AH information could underestimate the AH for the current simulations of 2016. The population in Singapore had increased from about 4.84 million in 2009 to about 5.61 million in 2016, a nearly 16% increment. AH emission could also have increased accordingly. However, the latest AH emission estimation is not available in open literature, and thus, the data by Quah and Roth (2012) were used for AH emission inputs in the current study. The UCM has about 20 urban input parameters, as listed in Table 3 along with their input values.

Table 3
Urban Parameters Used in UCM for Land Cover Categories

Parameters	LIR	HIR	C/I
Mean building height (m)	16.96	24.59	20.73
Standard deviation of building height (m)	14.46	20.13	21.71
Roof width (m)	22.33	26.12	51.76
Road width (m)	12.93	13.83	16.57
Heat capacity of roof ($\text{MJ m}^{-3} \text{K}^{-1}$)	1.20	1.20	1.20
Heat capacity of wall ($\text{MJ m}^{-3} \text{K}^{-1}$)	1.20	1.20	1.20
Heat capacity of road ($\text{MJ m}^{-3} \text{K}^{-1}$)	1.60	1.60	1.60
Thermal conductivity of roof ($\text{W m}^{-1} \text{K}^{-1}$)	0.67	0.67	0.67
Thermal conductivity of wall ($\text{W m}^{-1} \text{K}^{-1}$)	0.67	0.67	0.67
Thermal conductivity of road ($\text{W m}^{-1} \text{K}^{-1}$)	1.00	1.00	1.00
Albedo of roof	0.20	0.20	0.20
Albedo of wall	0.20	0.20	0.20
Albedo of road	0.10	0.10	0.10
Emissivity of roof	0.90	0.90	0.90
Emissivity of wall	0.90	0.90	0.90
Emissivity of road	0.95	0.95	0.95
Peak anthropogenic heat (AH) (W m^{-2})	13.00	18.00	113.00

2.2. General WRF Model Configuration

WRF version 3.8.1 coupled with single-layer UCM was used for the simulations in this study. Five nested domains, d01–d05, were configured, as shown in Figure 2a. The horizontal resolutions (grid points) of these domains are 24.3 km (76×76 , d01), 8.1 km (79×91 , d02), 2.7 km (112×112 , d03), 0.9 km (112×112 , d04), and 0.3 km (205×130 , d05), respectively. The innermost domain (d05) covers the area of interest, as shown in Figure 1.

In the vertical direction, 32 terrain-following eta levels were set from the land surface to the height of 40 hPa. The initial and boundary conditions for the model were deduced from NCEP GDAS/FNL 0.25° global tropospheric analyses and forecast grids (NCEP, 2015) at 6-hr temporal resolution. More details of the NCEP GDAS/FNL data can be found in

2.3. Sensitivity Test of WRF Physical Schemes

Major physical modules in WRF, including microphysics, cumulus, planetary boundary layer (PBL), and radiation modules, simulate the various processes in the atmosphere (such as cloud, rain, ice, snow, and graupel processes as well as the process of multiple bands, cloud, and cloud fraction effects from aerosols and trace gases). Proper selection of physical schemes for these modules is critical for the accuracy of urban climate simulation (Jandaghian et al., 2018). This part of study focuses on finding out the best combination of schemes for tropical urban climate simulation. For each of the physical modules, the more commonly used schemes were selected for the sensitivity test, which results in 12 simulation cases with different combination of physical schemes, as shown in Table 4.

Table 4

Setup of Simulation Cases for Sensitivity Study (Numbers Indicate the Option Codes in WRF)

Cases	Microphysics	Cumulus	PBL	Radiation	Cloud fraction
S01 ^a	Eta(5)	Kain-Fritsch(1)	MYJ(2)	Dudhia (1) + RRTMG(4)	Sundqvist(3)
S02	Kessler(1)	Kain-Fritsch(1)	MYJ(2)	Dudhia (1) + RRTMG(4)	Sundqvist(3)
S03	Goddard(7)	Kain-Fritsch(1)	MYJ(2)	Dudhia (1) + RRTMG(4)	Sundqvist(3)
S04	Eta(5)	Grell 3D (5)	MYJ(2)	Dudhia (1) + RRTMG(4)	Sundqvist(3)
S05	Eta(5)	Kain-Fritsch(1)	YSU(1)	Dudhia (1) + RRTMG(4)	Sundqvist(3)
S06	Eta(5)	Kain-Fritsch(1)	MYNN2(5)	Dudhia (1) + RRTMG(4)	Sundqvist(3)
S07	Eta(5)	Kain-Fritsch(1)	ACM2(7)	Dudhia (1) + RRTMG(4)	Sundqvist(3)
S08	Eta(5)	Kain-Fritsch(1)	MYJ(2)	RRTMG(24)	Sundqvist(3)
S09	Eta(5)	Kain-Fritsch(1)	MYJ(2)	CAM(3)	Sundqvist(3)
S10	Eta(5)	Kain-Fritsch(1)	MYJ(2)	New Goddard(5)	Sundqvist(3)
S11	Eta(5)	Kain-Fritsch(1)	MYJ(2)	GFDL(99)	Sundqvist(3)
S12	Eta(5)	Kain-Fritsch(1)	MYJ(2)	Dudhia (1) + RRTMG(4)	Xu-Randall(1)

^a Reference case.

Reasons for schemes selected for this sensitivity test are given in Supporting Information S2.

Case S01 was defined as the reference case consisting of a “reference” selection of physical schemes in each physics module. Selection of physical scheme in one of the five physics modules was then varied in each of the following cases to test the sensitivity on T2, wind and humidity predictions due to the variation of physical scheme selection relative to S01. Simulation results of all the 12 cases were compared with corresponding observation data obtained from the six weather stations listed in Table 1 to evaluate their accuracy. Simulations of all the 12 cases were conducted for the period indicated in Table 2 on the computational domain described in sections 2.1 and 2.2.

2.4. Evaluation Method

The error between simulation results and station observation data was evaluated by biased error (BE), as shown in Equation 1:

$$BE = R_m - R_o, \quad (1)$$

where R_m and R_o are simulation results and weather station observed data, both hourly, respectively. Number (N) of simulation result data points (for each of the output parameter—T2, RH, wind speed, or wind direction) that fall within a predefined error range around their corresponding observation data are then counted. The error range for T2 is $\pm 1^\circ\text{C}$, $\pm 10\%$ for RH, $\pm 1.5 \text{ m/s}$ for wind speed, and $\pm 45^\circ$ for wind direction. A hit ratio (HR) was then calculated to indicate the ratio of simulation result data points that are within the error range as compared to the total number of simulation result data points of the whole period (N_{all}) using

$$HR = \frac{N}{N_{all}} \times 100\%, \quad (2)$$

for each output parameter. For each simulation case, a combined hit ratio was calculated using

$$\text{Combined HR} = \frac{1}{3}HR_{T2} + \frac{1}{3}HR_{RH} + \frac{1}{6}HR_{windspeed} + \frac{1}{6}HR_{winddirection}. \quad (3)$$

The fractions multiplied to each individual HR on the right hand side of Equation 3 are weighting factors such that combined HR varies between 0% and 100%. The case that has the highest combined HR indicates the best combination of physical schemes. This best combination of physical schemes was then used in the subsequent UHI effect study and cool coating study.

Table 5
Albedo Value Setups for Cool Coating Study

Scenario	Albedo
Baseline	Roof = 0.20, wall = 0.20, road = 0.10
Cool_Surface	Roof = 0.88, wall = 0.88, road = 0.70
Cool_Roofs	Roof = 0.88, wall = 0.20, road = 0.10
Cool_Roads	Roof = 0.20, wall = 0.20, road = 0.70
Cool_Walls	Roof = 0.20, wall = 0.88, road = 0.10
Cool_Roof & Wall	Roof = 0.88, wall = 0.88, road = 0.10
Cool_Roof & Road	Roof = 0.88, wall = 0.20, road = 0.70
Cool_Road & Wall	Roof = 0.20, wall = 0.88, road = 0.70

and urban parameters shown in Table 3 were applied to the simulations.

2.6. Cool Coating Study

Net radiation on a surface, R_n , can be expressed by the surface radiation budget

$$R_n = SW_{in}(1 - \alpha) + LW_{in} + LW_{out}, \quad (4)$$

where SW_{in} the incoming short-wave radiation, α is albedo of the surface, and LW_{in} and LW_{out} are the incoming and outgoing long-wave radiations, respectively. Sleiman et al. (2011) and Li et al. (2013) suggested that high reflective urban surfaces can have albedo values up to 0.88. The change of urban surface albedo affects surface variables (temperature, heat flux, etc.) in the land surface model (LSM) in WRF and, thus, affects the PBL model that obtains boundary conditions from LSM.

This part of the study investigates the impact of large-scale application of cool coatings on the surfaces of urban structures in the area of interest to T2 and UHI intensity in Singapore. WRF-UCM simulations were conducted with different cool coating application scenarios, as summarized in Table 5, for the period indicated in Table 2 on the domain described in sections 2.1 and 2.2. General WRF model configuration shown in Table 2 and urban parameters shown in Table 3 were applied to the simulations, with the exception that the albedo values of urban surfaces were changed in different scenarios. The Baseline scenario represents the as-is (before cool coating application) situation with albedo values for roofs, walls, and roads set to the default value of 0.20, 0.20, and 0.10 in the model, respectively. In the other scenarios, cool coating was applied to the surfaces of roofs, walls, and roads individually or in combinations by changing the albedo value settings. Cool coated roofs were given an albedo value of 0.88 (Li & Norford, 2016). Cool coated roads were given an albedo value of 0.70, and cool coated walls were given an albedo value of 0.88. These values were taken from product information of cool coatings by a local supplier in Singapore. It is reported that cool materials could lose reflectance and, thus, the cooling effectiveness over time (Sleiman et al., 2011), but there have been continuous development in technologies, for example, self-cleaning properties and clear top coat, that aim to reduce the reflectance loss. The scenario “Cool_Surface” had cool coating applied to roofs, walls, and roads; that is, all urban structure surfaces were cool coated.

Simulation results in Singapore of each of the cool coating scenario were then compared with the Baseline scenario, to evaluate the impact of cool coating applied on roofs, walls, and roads across the land territories in the area of interest.

3. Results and Discussion

3.1. Sensitivity Study

The 12 simulation cases are evaluated with the combined HR method described in section 2.4, and the results are summarized in Table 6. S01 has the highest combined HR, suggesting that this combination of physical schemes has the best performance in predicting T2, wind, and RH prediction for the particular computational domain and period concerned in the current study.

Table 6
Hit Ratio and Combined Hit Ratio of the 12 Simulation Cases

Cases	T2	RH	Wind speed	Wind direction	Combined HR
S01	73.71%	86.71%	70.63%	68.45%	76.65%
S02	50.79%	83.63%	75.10%	60.71%	67.44%
S03	68.85%	85.42%	68.65%	66.17%	73.89%
S04	66.37%	80.26%	70.14%	67.96%	71.89%
S05	66.47%	83.43%	58.53%	63.29%	70.27%
S06	75.50%	84.62%	62.80%	65.08%	74.69%
S07	71.63%	78.97%	60.81%	59.33%	70.22%
S08	75.10%	87.00%	70.63%	63.59%	76.41%
S09	56.05%	87.90%	72.52%	69.44%	71.64%
S10	63.10%	87.90%	73.61%	71.13%	74.45%
S11	70.44%	84.92%	71.92%	68.85%	75.25%
S12	65.67%	83.93%	72.42%	70.63%	73.71%

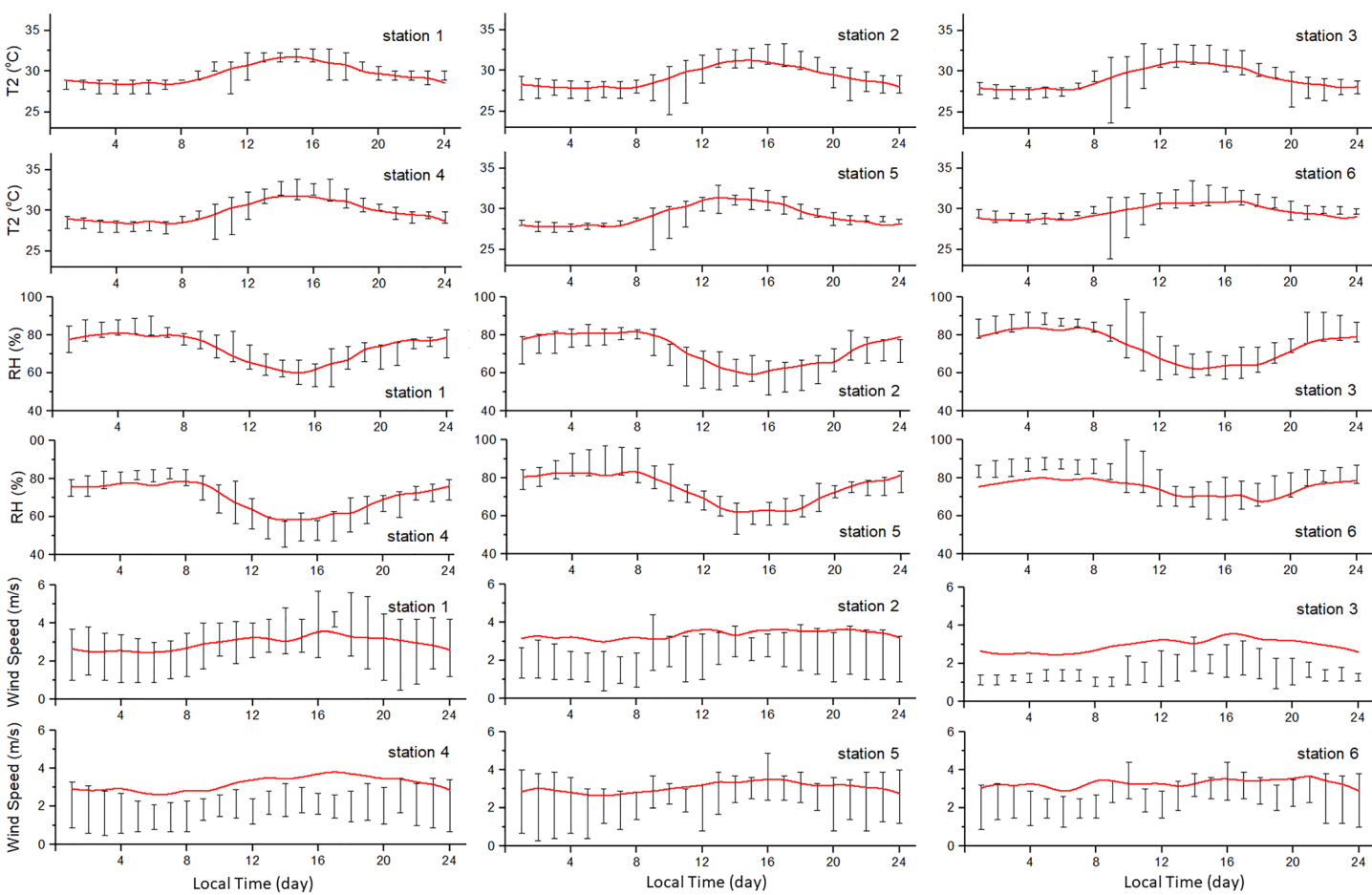


Figure 3. Comparison of the averaged T2, RH and wind speed (red line) of S01 from 2 to 7 Jul 2016 with the observed ranges at the six weather stations.

For S01, simulation results and station observation data are compared in the form of averaged diurnal profiles in Figure 3. The red line shows the hourly simulation results averaged across the 6-day simulation period (2–7 July 2016). The error bars show the maximum and minimum of observation data at each hour across the 6 days. The simulated averaged T2 and RH generally fall in the range of observation data, except for Station 6. This might be due to the coastal location of Station 6. The spatial resolution of the current WRF-UCM simulation is 0.3 km, suggesting that the simulation result at the coastal location of Station 6 could be highly impacted by the presence of sea surfaces in that pixel. This might lead to the consequence that the simulation results cannot follow the temporal variation in T2 and RH of observation data closely, due to the stabilizing effect on these parameters by the sea.

The average simulated wind speed at five out of the six stations is at the upper bound of the observation range, indicating that wind speed is generally overestimated by the simulations. In UCM, urban geometry is represented by urban canopy, and thus, individual building characteristics, height distribution, and orientation, which could change the roughness of urban canopy value, are not considered. UCM parameterizes urban structures with a uniform set of building height, roof width, road width, AH, and other physical parameters of the building envelope, including heat capacity, thermal conductivity, surface albedo, and thermal emissivity. With this parametrization, the urban canopy representation has a much lower roughness than the real urban topology. However, actual wind speed measurements in weather stations are affected by actual urban topology. This could contribute to the general overestimation of wind speed by WRF-UCM.

Sensitivity study of the 12 cases using mean bias error (MBE) and root-mean-square error (RMSE) is given in Supporting Information S2 and S3. The study also shows that S01 is the best combination. Time series

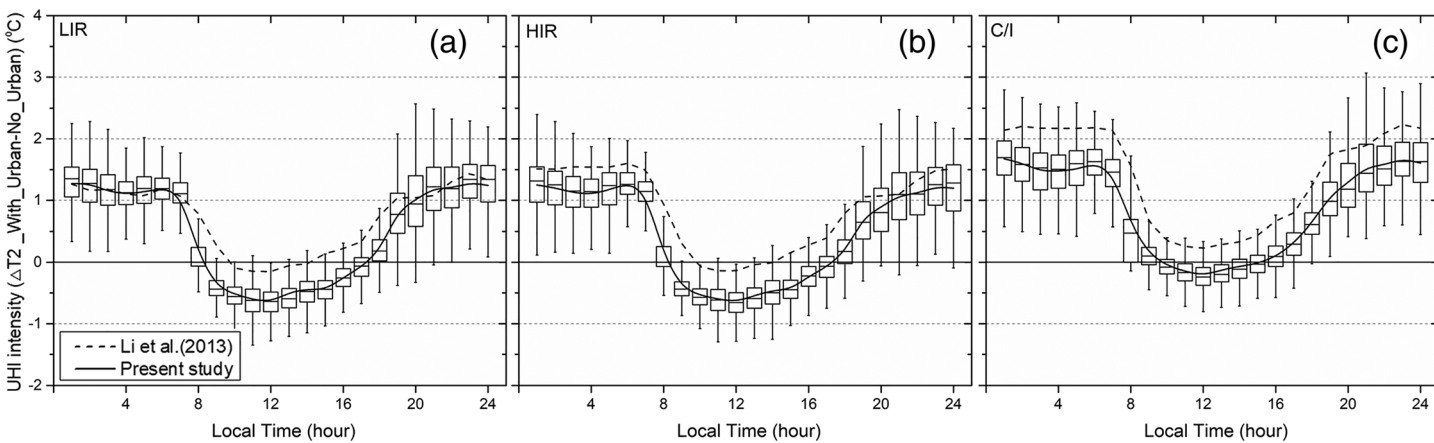


Figure 4. Averaged UHI intensity ($T_2\text{with}_{\text{Urban}} - T_2\text{No}_{\text{Urban}}$) in (a) LIR area, (b) HIR area, and (c) C/I area for 2 to 7 July 2016.

comparison between simulation results of S01 and observation data without averaging is also given in Supporting Information S3 for reference.

3.2. UHI Effect in Singapore

The temporal profiles of UHI intensity ($T_2\text{with}_{\text{Urban}} - T_2\text{No}_{\text{Urban}}$) of the three urban land use categories in Singapore are shown in Figure 4 (solid lines). Each hourly UHI intensity data point for a land use category was averaged across all pixels in that category and across 6 days of predictions (2–7 July 2016), that is, the data point for 01:00 is the average of all 01:00 results of the 6 days. Each box plot shows the distribution of results for each hour across all pixels of that land use category and in the same hour of the 6 days. The simulation results reported by Li et al. (2013) are also plotted in Figure 4 for comparison.

High UHI intensities are found during nighttime (20:00–07:00) whereas low UHI intensities, or even urban cool island (UCI), are found during daytime (08:00–19:00). Averaged UHI intensity during nighttime varies between 1°C and 2°C, with a maximum of 3.2°C found in certain locations in C/I area. It could be inferred from Figure 2c that the UHI intensity profiles have an inverse correlation with the global horizontal irradiance (GHI) intensity profile. During nighttime, when there is no GHI, the main contributing factors to UHI are AH and the release of stored heat from urban structures. Figure 2c shows that AH are at lower values during nighttime compared to those during daytime. From 20:00–24:00, AH shows a sharp drop, but the UHI intensities continue to increase during this period. It suggests that the release of stored heat from urban structures is a dominating factor to UHI effect.

The temporal profiles of UHI intensity obtained in the present study show similarity with those reported in Li et al. (2013), that is, high UHI intensity during nighttime and low UHI intensity during daytime with occurrence of UCI. UHI intensities obtained in the present study are, in general, slightly lower (by less than 0.5°C) than those in Li et al. (2013). The discrepancy could be attributed to the difference in simulation period (2007/2008 in Li et al. (2013)) and land use map between the two studies. The average urban fraction among all HIR 90-m pixels is 62.60%, LIR is 66.03%, and C/I is 73.85% in present study whereas fixed urban fraction values of 0.8, 0.7, and 0.95 were assigned to all HIR, LIR, and C/I pixels, respectively, in Li et al.'s (2013) study. Chow and Roth (2006) reported that a maximum UHI of 7°C was found in Singapore, which was based on measurements at five stations. Nevertheless, Chow and Roth (2006) also reported the occurrence of UCI during daytime in Singapore.

The causes of UHI effect can be further analyzed using surface energy balance as expressed by

$$Q_N + AH = Q_H + Q_E + G + Q_A, \quad (5)$$

where Q_N is the net downward radiative flux (longwave + shortwave), AH is the anthropogenic heat flux, Q_H is the upward sensible heat flux, Q_E is the upward surface latent heat flux due to evaporation, Q_A is the

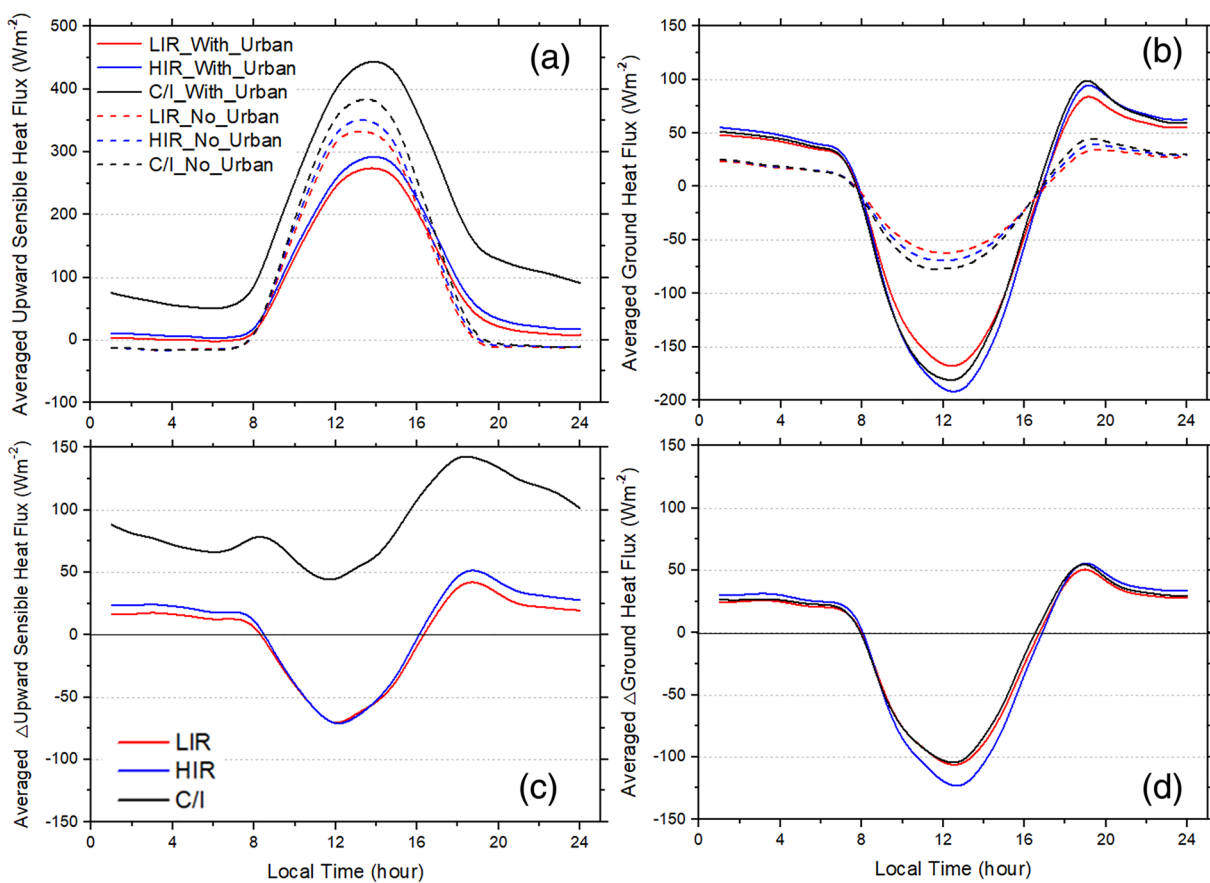


Figure 5. Averaged (a) Q_H , (b) G , (c) ΔQ_H , and (d) ΔG for 2 to 7 July 2016. $\Delta = \text{With}_\text{Urban} - \text{No}_\text{Urban}$.

net horizontal heat advection, and G is the ground heat flux into the subsurface medium and urban structures (in case of having urban) (Mayocchi & Bristow, 1995).

Temporal profiles of averaged Q_H and G are shown in Figures 5a and 5b. Spatial-temporal averaging similar to that in Figure 4 is applied here. Figure 5a shows that Q_H is positive for almost the entire day (daytime and nighttime) in the With_Urban scenario, but there is a clear distinction of positive Q_H during daytime and negative Q_H during nighttime in the No_Urban scenario. The positive Q_H during daytime is largely due to the heating of land mass (No_Urban) and urban structures (With_Urban) by incoming radiative flux. In the With_Urban scenario, there is an additional contribution to Q_H by AH. This can be clearly seen in C/I, which has much higher AH than the other two residential categories. In LIR and HIR, Q_H during daytime is less with urban than with no urban, despite the contribution by AH. It suggests that the heat absorption effect of urban structures during daytime might have outweighed the contribution by AH in these two categories. Heat absorption by urban structure could also be happening in C/I, but apparently, it does not outweigh the AH due to the much higher AH in C/I.

The heat absorption effect of urban structures can be seen more clearly in G (Figure 5b). G is negative during daytime in both scenarios, indicating heat absorption by land mass (No_Urban) and urban structures (With_Urban). The magnitudes of negative G in the With_Urban scenario are much higher than those in the No_Urban scenario during daytime, indicating the additional heat absorption effect by urban structures in all three urban categories. The heat absorption effect by urban structures could be a major contributor to the reduction of UHI intensity and the occurrence of UCI during daytime, as indicated in Figure 4. G is positive during nighttime in both scenarios, suggesting that there is release of stored heat by land mass (No_Urban) and urban structures (With_Urban). The With_Urban scenario has more heat released than the No_Urban scenario, which indicates the additional heat release by urban structures during nighttime.

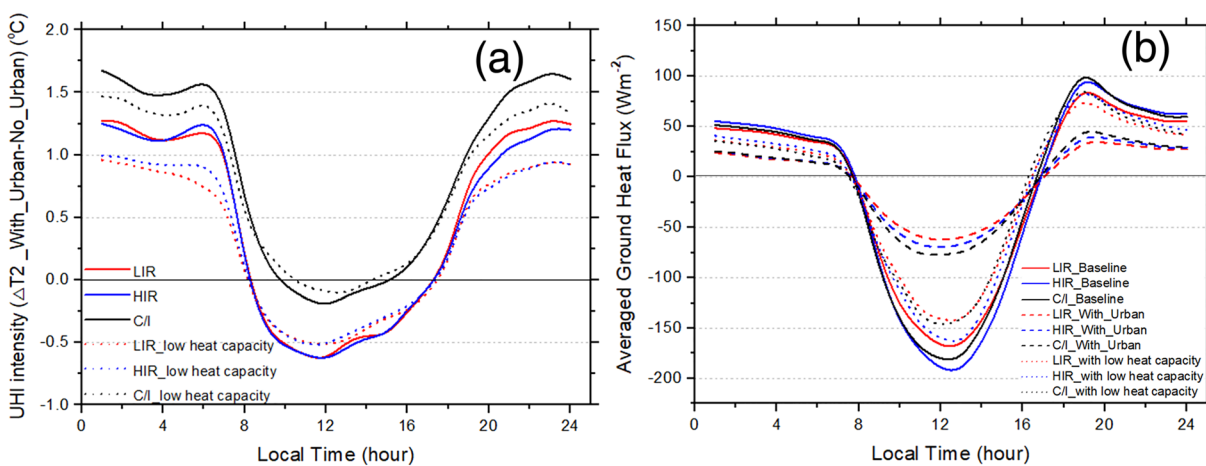


Figure 6. Averaged (a) UHI intensity ($T_2^{\text{With_Urban}} - T_2^{\text{No_Urban}}$) and (b) G in Baseline and with low heat capacity.

as a result of more heat absorption during daytime. This contributes to the high UHI intensities found during nighttime (Figure 4).

The impact of AH, as compared to urban structure heat absorption/release, on UHI intensity can be shown more clearly by the difference in Q_H between the With_Urban and No_Urban scenarios (Figure 5c). In C/I, which has much higher AH than the other two categories, ΔQ_H , is positive throughout the whole day despite the heat adsorption by urban structures during daytime. This gives rise to the fact that the UCI intensity in C/I is much less than that in LIR and HIR (Figure 4). UHI intensity in C/I is roughly 0.5°C higher than LIR and HIR throughout the day, indicating the contribution by the higher AH in C/I. ΔQ_H in LIR and HIR becomes negative during daytime indicating that the additional heat absorption effect by urban structures outweighed AH in these areas. ΔG (Figure 5d) gives a direct indication of the heat absorption/release effect by urban structures. Its temporal profile largely resembles the profile of UHI intensity, suggesting that the heat absorption/release effect by urban structures contributes significantly to UHI effect. In Figures 5b and 5d, the G in the With_Urban cases has lower values than in the No_Urban case during daytime, indicating the heat absorption of buildings contributed to UCI. The G of HIR is lower than that of LIR, suggesting that the urban structures in HIR absorb more energy, due to higher density of buildings, than those in LIR.

For the property of buildings, we conducted an additional case in which the heat capacities of roof and wall were halved ("low heat capacity" in Figure 6). The results show that halving the heat capacity of building structures leads to reduced heat absorption (Figure 6b) during daytime reducing the UCI intensity during daytime (Figure 6a). Halving the heat capacity of building structures also leads to less heat release during nighttime, contributing to lower UHI intensity during nighttime. The results indicate the connection between urban structure heat absorption/release and UCI/UHI.

Figure 7 shows the spatial distributions of averaged T_2 in the area of interest at 01:00 (nighttime) and 13:00 (daytime). The T_2 value shown on each pixel is averaged across 6 days of predictions (2–7 July 2016) for the same hour that is being shown. As seen from Figure 7a, the urban areas generally have higher T_2 than rural areas during nighttime, suggesting that the release of stored heat from urban structures is a significant cause of nocturnal UHI effect, as described above. The spatial distribution of averaged UHI intensity during nighttime (Figure 7c) is also highly correlated to high-intensity urban areas. The spatial correlation between high T_2 and urban areas is much less obvious during daytime than nighttime, as shown in Figure 7b. This could be because both the urban and rural areas are subjected to heating by incoming solar radiation during daytime. The heat absorption by urban structures could offset part of that heating in urban areas whereas such offsetting mechanism do not exist in rural area, leading to low (or even negative) UHI intensity. Instead of the highly urbanized areas along the southern coast, peak T_2 values are found at the northern part of Singapore, which could more likely be caused by the southerly wind (prevailing for the simulated period) that carries the urban heat toward the north. UHI intensity distribution during daytime (Figure 7d) also show less correlation with the urban areas than that during the nighttime (Figure 7c). This, again, suggests that release of stored heat from urban structure is a major cause of UHI during nighttime.

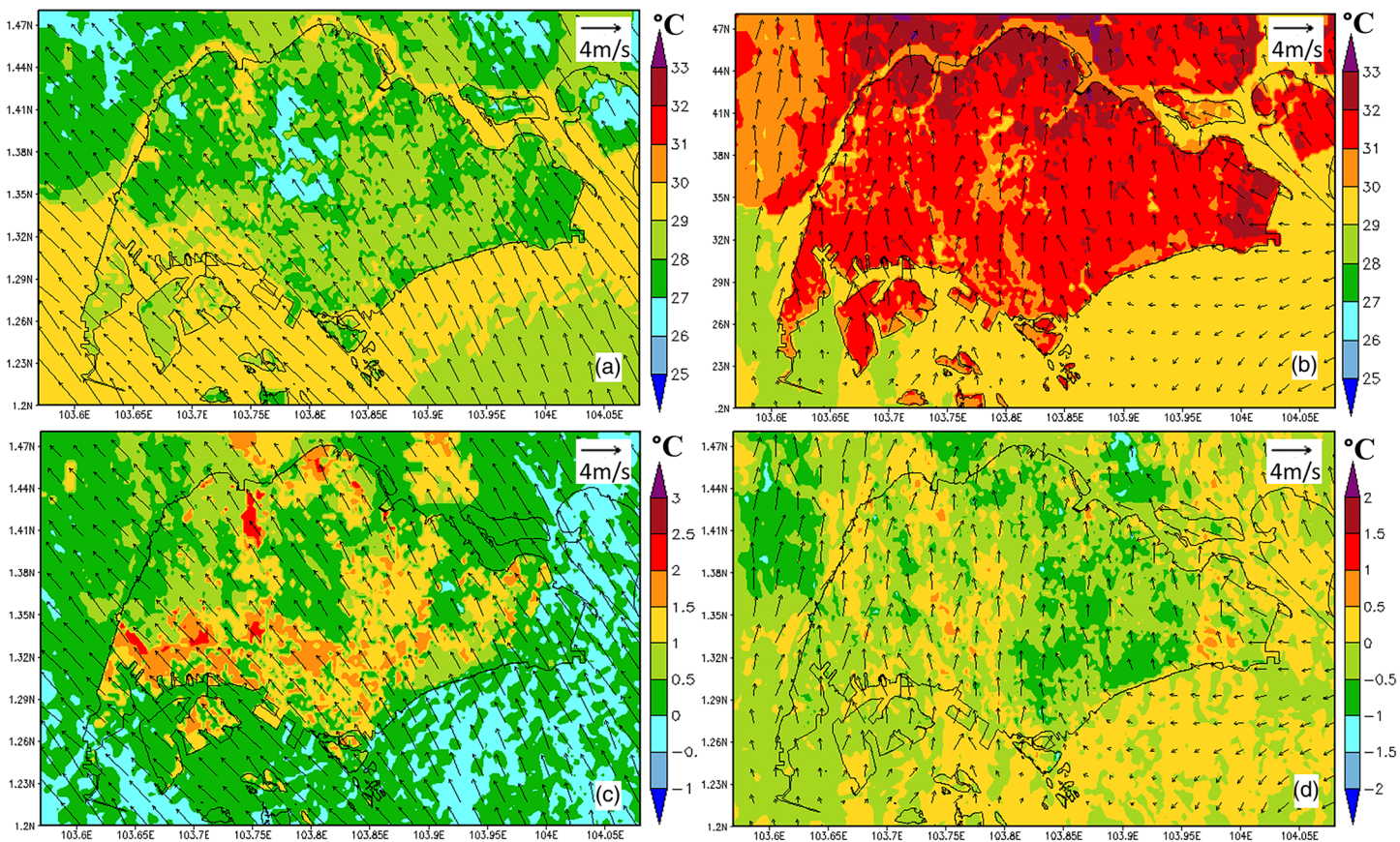


Figure 7. Averaged T2 at (a) 01:00 LT, (b) 13:00 LT, and averaged UHI intensity ($T_2\text{With_Urban} - T_2\text{No_Urban}$) at (c) 01:00 LT, (d) 13:00 LT for 2 to 7 July 2016. Wind velocity vectors at 10-m elevation from surface are shown (unit: m/s).

3.3. Cool Coating Effects

3.3.1. Urban Cooling by Cool Coatings

The spatial-temporal averaged ΔT_2 and ΔT_{SK} between the Baseline and Cool_Surface scenarios are plotted in Figure 8. The same spatial-temporal averaging as shown in section 3.2 is adopted here, that is, averaged across all pixels in each land use category and across 6 days of predictions (2–7 July 2016). Since $\Delta = \text{Baseline} - \text{Cool_Surface}$, thus a positive value in Figure 8 indicates the cooling effect of applying cool

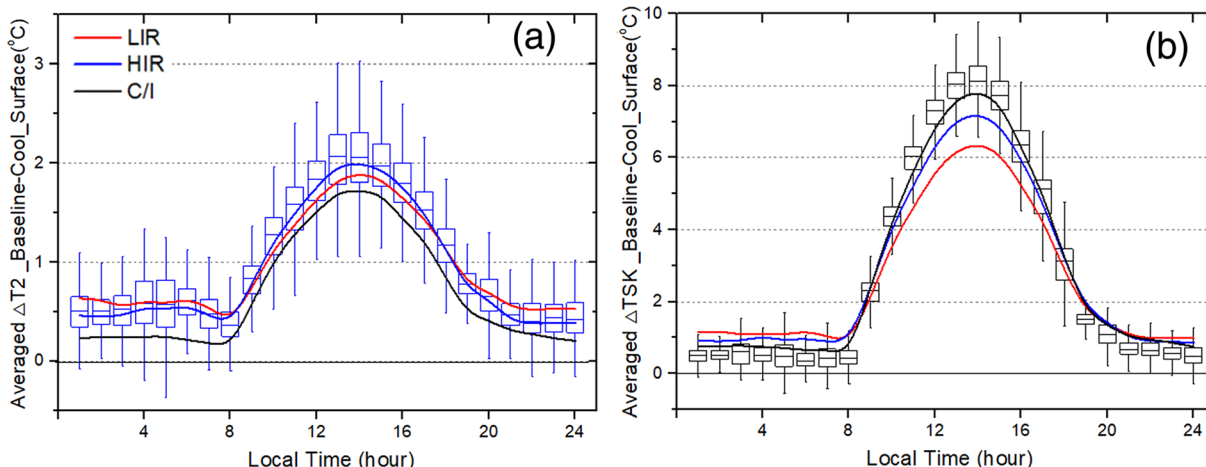


Figure 8. Averaged ΔT_2 (a) and ΔT_{SK} (b) between the Baseline and Cool_Surface scenarios for 2 to 7 July 2016. $\Delta = \text{Baseline} - \text{Cool_Surface}$.

Table 7

Areas and Percentages of Each Cool Coating Surfaces in Each Urban Category Pixel

Type of surfaces	LIR		HIR		C/I	
	km ²	% ^a	km ²	% ^a	km ²	% ^a
Roofs	16.16	63.33	21.58	65.38	29.25	75.75
Walls	24.55	-	40.63	-	23.44	-
Roads	9.36	36.67	11.42	34.62	9.37	24.25

^a Percentage of horizontal plane area covered as compared to total horizontal plane area of each urban pixel.

coating on all urban surfaces. Box plots are shown for the land use category that reaches the highest value among the three categories, to show the distribution of results for each hour across all pixels of that land use category and in the same hour of the 6 days. The box plots of all three categories are given as Figure S1-1.

Figure 8 shows that the Cool_Surface scenario has cooling effect in the urban areas compared to the Baseline scenario throughout the whole day. The cool coating effect, as reflected by averaged ΔT_2 , in the residential areas (LIR & HIR) is about 0.5°C and about 0.2°C in C/I during nighttime (20:00–07:00). The cooling effect increases with the GHI intensity from 08:00 onwards and reaches a maximum at around 14:00. The cooling effect then drops following the decline of GHI till 20:00, when the sun is

fully set. The most significant cooling effect happens from 13:00 to 15:00, during which the averaged ΔT_2 in HIR reaches 2.0°C, with a maximum value of 3.1°C. However, the highest averaged ΔT_{SK} is found in C/I, reaching 7.9°C with a maximum value of 9.8°C. C/I has the highest roof density (as shown in Table 7) and the largest ΔT_{SK} among the three urban categories since ΔT_{SK} is a direct indication of surface cooling effect due to cool surfaces. It suggests that ΔT_2 is subjected to influences from more factors (wind, AH, etc.) than ΔT_{SK} .

The impact of cool coating on urban cooling can be further analyzed through urban surface energy balance. Figure 9a shows the averaged Q_H of the Baseline and Cool_Surface scenarios and the ΔQ_H of the two scenarios is shown in Figure 9c. Since Q_H in urban area represents the sensible heat release from urban surface to the ambient, the difference in Q_H between the two scenarios can give a direct indication of reduced heat release by urban structures to the ambient due to application of cool coating. The Cool_Surface scenario

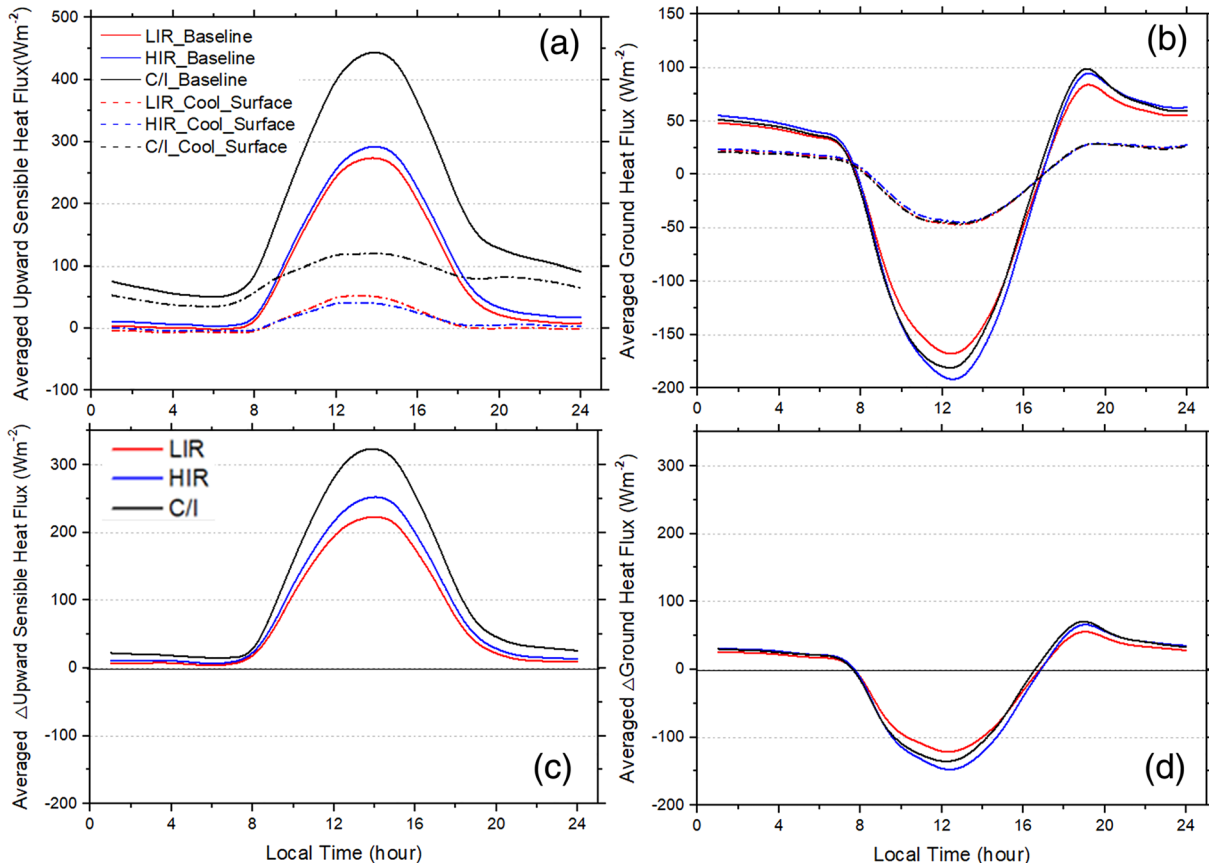


Figure 9. Averaged (a) Q_H , (b) G , (c) ΔQ_H , and (d) ΔG for 2 to 7 July 2016. Δ = Baseline – Cool_Surface.

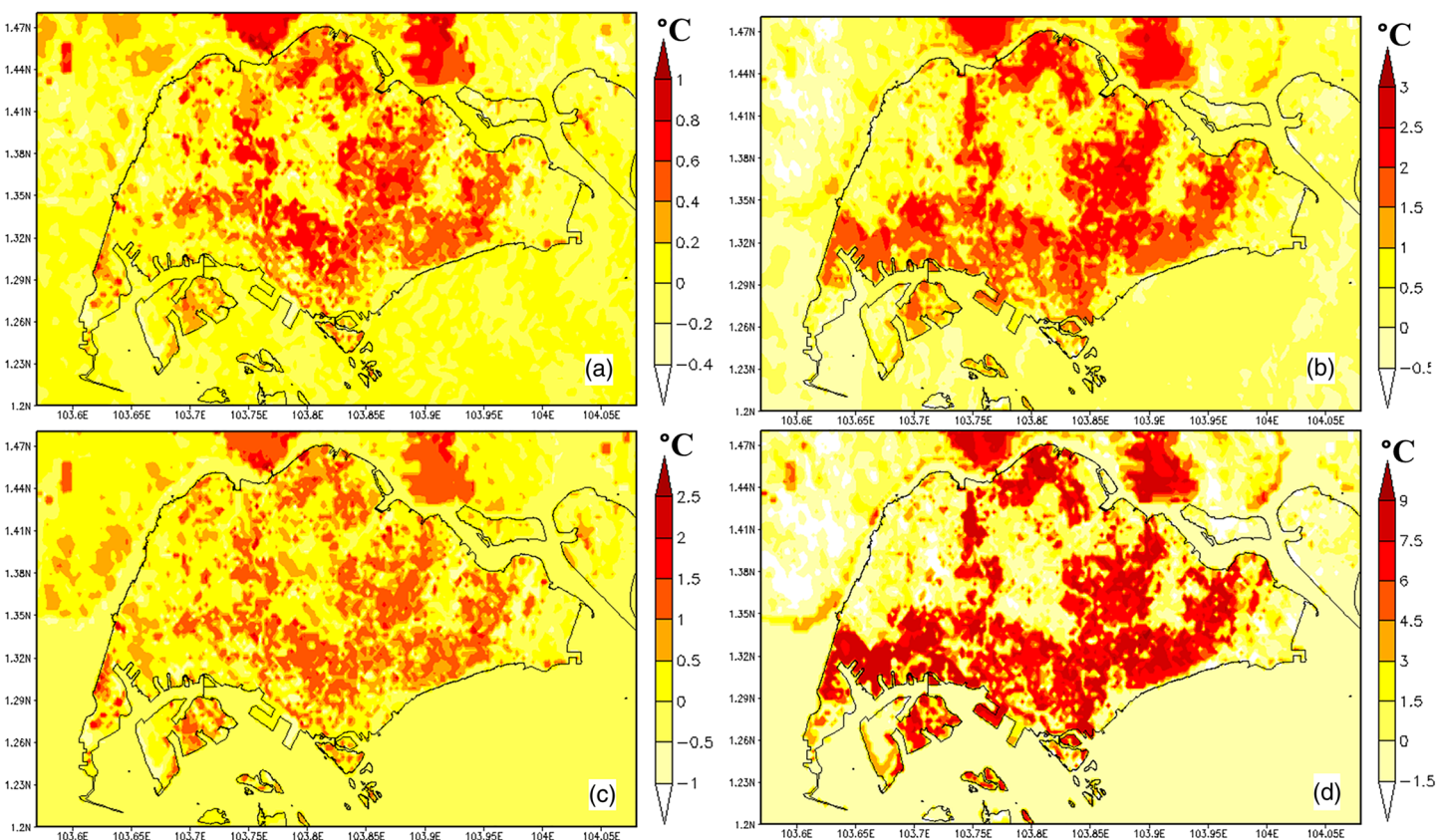


Figure 10. Averaged ΔT_2 at (a) 01:00 LT, (b) 13:00 LT and ΔT_{SK} at (a) 01:00 LT, (b) 13:00 LT for 2 to 7 July 2016. $\Delta = \text{Baseline} - \text{Cool_Surface}$.

provides positive Q_H reduction effect, as compared to Baseline, throughout the whole day (daytime and nighttime) as indicated by Figure 9c. Q_H reduction by Cool_Surface is much more significant during daytime compared to nighttime. This could be due to the fact that the higher albedo surfaces reduce radiative heat absorption by urban structures during daytime, leading to reduced sensible heat release by urban structures. In contrast, during nighttime, there is no GHI, and thus, the cool coating effect on reducing radiative heat absorption by urban structures does not exist. Q_H reduction by Cool_Surface during nighttime could mainly be attributed to the reduced heat storage in urban structures, as the cool surfaces reduce radiative heat absorption during the day. This is evident in Figure 9d that ΔG during daytime is negative (reduced radiative heat absorption in Cool_Surface scenario) and is positive (reduced heat release in Cool_Surface scenario) during nighttime.

Figure 9a also reveals that Q_H in C/I is much higher than LIR and HIR throughout the whole day, in both scenarios. This indicates the contribution of urban heating by AH. Cool urban surfaces could reduce urban heating due to heat absorption by and subsequent release from urban structures but have no impact to AH, in the way of AH treatment in the present study. This can be seen from Figure 9a that, in the Cool_Surface scenario, Q_H in C/I remains much higher than LIR and HIR throughout the whole day despite the cool coating effect. Define a nocturnal UHI mitigation efficiency ($MUHI_{noc}$) for each urban land use category as

$$MUHI_{noc} = \frac{\Delta T_{2CoolSurface}}{UHI} | 2000 - 0700 \times 100\%, \quad (6)$$

where the $\Delta T_{2CoolSurface}$ is ΔT_2 in the Cool_Surface scenario and UHI is the UHI intensity. The equation is averaged across the nighttime hours (20:00–07:00 LT). Using this definition, high-albedo urban surfaces provide 38.1% of $MUHI_{noc}$ in LIR followed by 29.9% in HIR. $MUHI_{noc}$ is largely reduced to 5.8% in C/I,

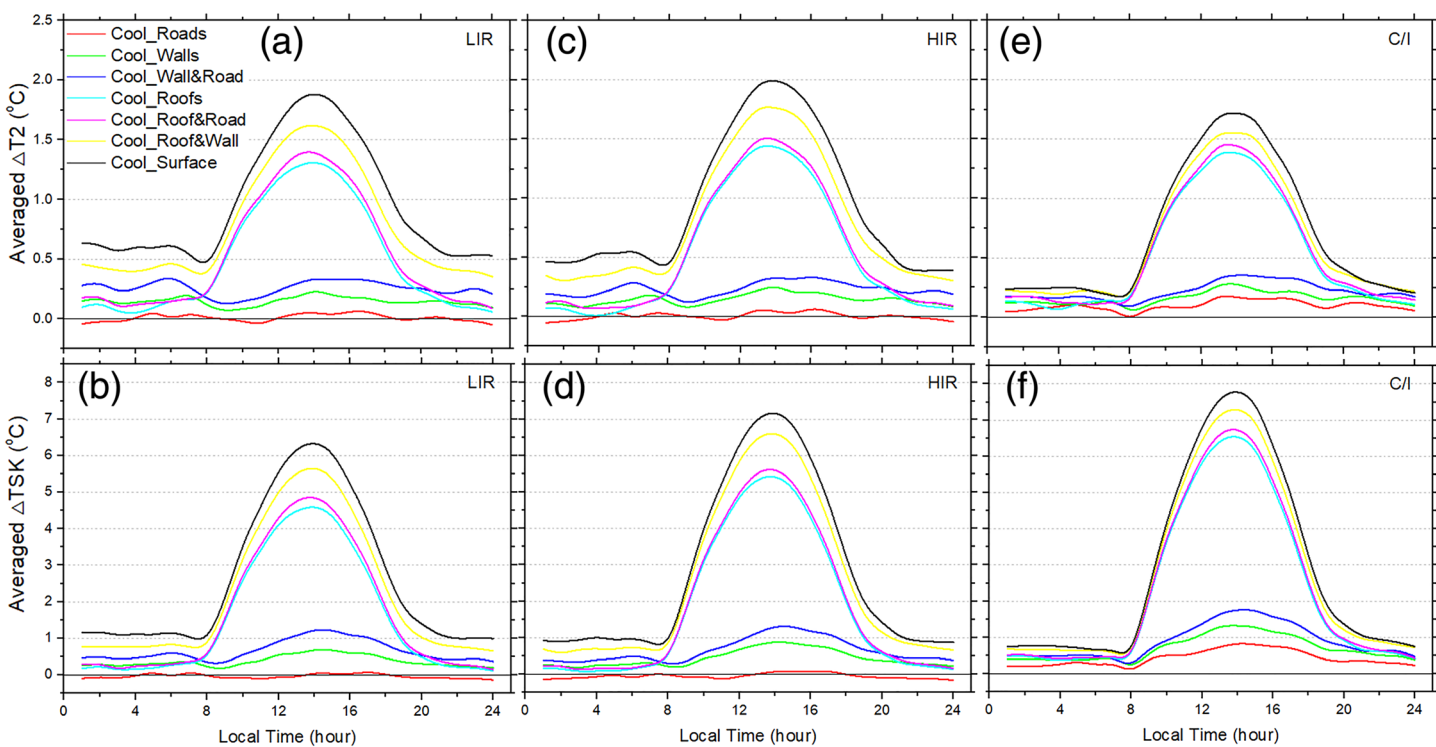


Figure 11. Averaged ΔT_2 and ΔT_{SK} for different cool coating scenarios in (a,b) LIR, (c,d) HIR, and (e,f) C/I area for 2 to 7 July 2016. Δ = Baseline – Cool coating scenarios.

suggesting that high-albedo urban surfaces are less effective in mitigating nocturnal UHI in urban areas that have high AH.

Spatial distributions of cooling effects due to cool surfaces in terms of averaged ΔT_2 and averaged ΔT_{SK} are shown in Figure 10, respectively. Spatial distributions of ΔT_{SK} highly match with the locations of the urban areas since ΔT_{SK} is a direct indication of surface cooling effect due to cool surfaces. Significant ΔT_2 generally occurs in urban areas as well, indicating the UHI mitigation effect of cool surfaces. The spatial distribution of ΔT_2 could be slightly spread and offset from the urban areas.

3.3.2. Cool Coating Effect on Different Types of Urban Surfaces

Impact of applying cool coating on individual type of urban surfaces (roofs, walls, and roads) on urban cooling as measured by averaged ΔT_2 and ΔT_{SK} is shown in Figure 11. Among the three types of surfaces, Cool_Roofs provide the most significant cooling effect followed by Cool_Walls. Despite being all horizontal surfaces (same as roofs), Cool_Roads provide the least significant cooling effect. This could be because Roads in the current land use map comprises road surfaces within the urban pixels, and thus, the solar access of road surfaces could be limited by surrounding buildings. The total surface area of Roads is the least amount of the three types of surfaces, about half of the area of Roofs and one-third of the area of Walls. Part of the reflected radiation from Roads could also end up being absorbed by surrounding buildings instead of escaping the canopy layer, reducing the cooling effect of Cool_Roads. This could be somewhat mitigated by putting cool coatings on both the roads and the walls. However, this is still less effective than putting cool coating on Roofs alone. The reflected radiation from Cool_Roofs can escape the canopy layer freely, leading to high cooling effect by Cool_Roofs. Cool_Roofs provide cooling effect of up to 1.4°C averaged ΔT_2 and 6.8°C averaged ΔT_{SK} during 13:00–15:00, similar to those reported by Li et al. (2013). In addition to Cool_Roofs, adding cool coating on any other type of surface will enhance the cooling effect. Applying cool coating on all three types of surfaces will provide the highest cooling effect among all cool coating scenarios, reaching 2.0°C in averaged ΔT_2 and 7.9°C in averaged ΔT_{SK} during 13:00–15:00.

Besides T2 and TSK, the impact of cool coating on human thermal sensation can be investigated through Heat Index (HI), which is a measure of human thermal sensation when RH is factored into the

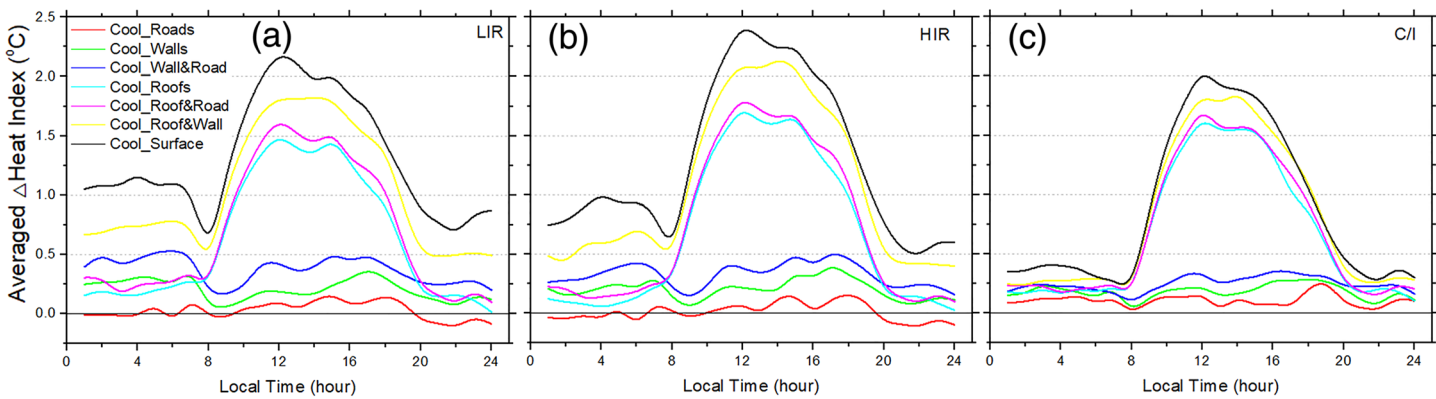


Figure 12. Averaged Δ heat index for different cool coating scenarios in (a) LIR, (b) HIR, and (c) C/I area (e,f) from 2 to 7 July 2016. Δ = Baseline – Cool coating scenarios.

consideration. HI is computed by a model based on multiple regression analysis proposed by National Weather Service (NWS) (1990), which is

$$\begin{aligned} \text{HI} = & -42.38 + 2.05T + 10.14\text{RH} - 0.22 \cdot T \cdot \text{RH} - 6.84 \times 10^{-3} \cdot T^2 - 0.05\text{RH}^2 \\ & + 1.23 \times 10^{-3} \cdot T^2 \cdot \text{RH} + 8.53 \times 10^{-4} \cdot T \cdot \text{RH}^2 - 1.99 \times 10^{-6} T^2 \cdot \text{RH}^2, \end{aligned} \quad (7)$$

where T is air temperature in °F (using T_2 in this paper) and RH is in %. For $\text{RH} > 85\%$ and $80 \leq T \leq 87$ °F, the following adjustment is made to HI:

$$\text{HI} = \text{HI} + \left[\frac{\text{RH} - 85}{10} \right] \times \left[\frac{87 - T}{5} \right]. \quad (8)$$

In this paper, the final calculated HI is expressed in °C.

The impact of applying cool coating on individual urban surfaces (roofs, walls, and roads) as measured by averaged Δ HI is shown in Figure 12. HI reduces by about 2°C across the urban areas at noon time in the Cool_Surface scenario. Highest HI reduction is seen in the HIR area, reaching 2.4°C at noon time. The results indicate the effect of applying cool coating in improving pedestrian comfort in the urban environment.

Due to the resolution of mesoscale modeling WRF-UCM, it cannot capture the details of building characteristics, for example, individual building height, AH of each building, and window-to-wall ratios so as to resolve the actual air temperature down to street level. These parameters will be updated and coupled with microscale simulation. Due to the limitation of simulation period (early July in southeasterly monsoon season), the present study did not investigate into the effect of cool coating on atmospheric conditions and the seasonal effect on UHI and cool coating effect. These issues will be addressed in the followed studies.

4. Conclusions

Mesoscale meteorological modeling using Weather Research and Forecasting (V3.8.1) coupled with UCM (WRF-UCM) was conducted to evaluate T_2 , wind speed/direction, and RH in Singapore, a tropical city, for a dry summer period in 2016. A sensitivity study was conducted to determine the best combination of schemes for the physical models. Each combination was evaluated based on the errors in model predictions as compared to observations from six weather stations across Singapore. Out of the 12 tested combinations, the best combination of Eta microphysics scheme, Kain-Fritsch cumulus scheme, MYJ planetary boundary layer (PBL) scheme, Dudhia radiation scheme, and Sundqvist cloud fraction scheme was selected.

WRF-UCM simulations using the best combination of schemes were conducted to study the UHI effect and urban cooling effect by applying cool coating on urban structure surfaces in Singapore for this summer dry period. UHI effect is more intense during nighttime, compared to daytime. Nocturnal averaged UHI intensity in urban areas varies between 1°C and 2°C, reaching up to a maximum of 3.2°C at certain locations in

C/I area. Release of heat stored in urban structures due to absorption of incoming solar radiation and anthropogenic heat are two main contributors to the nocturnal UHI effect.

The impact of applying cool coating on the surfaces of urban structures (roofs, walls, and roads) to urban T2 and TSK in Singapore was studied by WRF-UCM simulations. Applying cool coating on all urban surfaces can reduce the averaged T2 and surface skin temperature (TSK) by up to 2.0°C and 7.9°C. Maximum T2 reduction of 3.1°C and TSK reduction of 9.8°C is found at certain locations. The higher albedo cool urban surfaces reduce radiative heat absorption by urban structures during daytime, which reduces heat storage in urban structures, leading to subsequent reduction of release of stored heat from urban structures, mitigating UHI effect during nighttime. However, since the anthropogenic heat is another major contributing factor to UHI effect, the effect of cool coating on mitigating UHI effect is less significant in areas with high anthropogenic heat than areas with low anthropogenic heat. The current results show that cool coating can provide nocturnal UHI mitigation efficiency of 30–38% in residential areas but only about 6% in commercial/industrial areas, which has much higher anthropogenic heat than residential areas. It indicates that cool coating as an urban cooling measure is more effective in areas having low anthropogenic heat (e.g., residential area) than in areas having high anthropogenic heat (e.g., commercial area). Additional heat mitigation methods might need to be considered in high anthropogenic heat areas.

Simulations of applying cool coating on individual type of urban surfaces (roofs, walls, and roads) show that cool roofs provide the most significant cooling effect among the three types of surfaces, followed by cool walls and cool roads. The reflected radiation from roofs can escape the canopy layer freely, leading to high cooling effect. In contrast, the solar access of road surfaces could be limited by surrounding buildings. Part of the reflected radiation from Roads could also end up being absorbed by surrounding buildings instead of escaping the canopy layer, reducing the cooling effect of cool roads. This could be somewhat mitigated by putting cool coatings on both the roads and the walls. Applying cool coating on all urban surfaces provides the most significant urban cooling effect.

Data Availability Statement

The satellite data were provided by Geoscience Consulting Pte Ltd in Singapore. NCEP GDAS/FNL 0.25 Degree Global Tropospheric Analyses and Forecast Grids data were obtained from the NCEP website (<https://rda.ucar.edu/datasets/ds083.3/index.html>).

Acknowledgments

This research is supported in part by the Singapore Ministry of National Development and the National Research Foundation, Prime Minister's Office under the Land and Liveability National Innovation Challenge (L2 NIC) Research Programme (L2 NIC Award No L2NICCFP2-2015-4). Any opinions, findings, and conclusions or recommendations expressed in this material are those of the author(s) and do not reflect the views of the Singapore Ministry of National Development and National Research Foundation, Prime Minister's Office, Singapore. Zhou Mandi and Long Yongping contributed equally to this work. The observations in Singapore were supported by the Meteorological Service Singapore (<http://www.weather.gov.sg/>).

References

- Central Intelligence Agency (2018). World Factbook Urbanization. Retrieved from: <https://www.cia.gov/library/publications/the-world-factbook/fields/2212.html>
- Chen, F., Kusaka, H., Bornstein, R., Ching, J., Grimmond, C. S. B., Grossman-Clarke, S., & Zhang, C. (2011). The integrated WRF/urban modelling system: Development, evaluation, and applications to urban environmental problems. *International Journal of Climatology*, 31(2), 273–288. <https://doi.org/10.1002/joc.2158>
- Ching, J., Brown, M., Burian, S., Chen, F., Cionco, R., Hanna, A., et al. (2009). National urban database and access portal tool. *Bulletin of the American Meteorological Society*, 90(8), 1157–1168. <https://doi.org/10.1175/2009BAMS2675.1>
- Chow, W. T. L., & Roth, M. (2006). Temporal dynamics of the urban heat island of Singapore. *International Journal of Climatology*, 26(15), 2243–2260. <https://doi.org/10.1002/joc.1364>
- Energy Market Authority of Singapore (2016). Singapore Electricity Market Outlook. Retrieved from: <https://www.ema.gov.sg/cmsmedia/Singapore%20Electricity%20Market%20Outlook%20Final.pdf>
- EOPortal (2014). TanDEM-X: TerraSAR-X add-on for Digital Elevation Measurement, Retrieved from <https://directory.eoportal.org/web/eoportal/satellite-missions/t/tandem-x>
- Meteorological Service Singapore (2012). The weather and climate of Singapore. Retrieved from: <https://www.nea.gov.sg/corporate-functions/resources/publications/books-journals-and-magazines/weather-and-climate-of-singapore>
- Georgescu, M., Morefield, P. E., Bierwagen, B. G., & Weaver, C. P. (2014). Urban adaptation can roll back warming of emerging megapolitan regions. *Proceedings of the National Academy of Sciences*, 111(8), 2909–2914. <https://doi.org/10.1073/pnas.1322280111>
- Hajat, S., Vardoulakis, S., Heaviside, C., & Eggen, B. (2014). Climate change effects on human health: Projections of temperature-related mortality for the UK during the 2020s, 2050s and 2080s. *Journal of Epidemiology and Community Health*, 68(7), 641–648. <https://doi.org/10.1136/jech-2013-202449>
- Heaviside, C., Macintyre, H., & Vardoulakis, S. (2017). The urban heat island: Implications for health in a changing environment. *Current Environmental Health Reports*, 4(3), 296–305. <https://doi.org/10.1007/s40572-017-0150-3>
- Jandaghian, Z., Touchaei, A. G., & Akbari, H. (2018). Sensitivity analysis of physical parameterizations in WRF for urban climate simulations and heat island mitigation in Montreal. *Urban Climate*, 24, 577–599. <https://doi.org/10.1016/j.uclim.2017.10.004>
- Kardinal Jusuf, S., Wong, N. H., Hagen, E., Anggoro, R., & Hong, Y. (2007). The influence of land use on the urban heat island in Singapore. *Habitat International*, 31(2), 232–242. <https://doi.org/10.1016/j.habitatint.2007.02.006>
- Kovats, R. S., & Hajat, S. (2008). Heat stress and public health: A critical review. *Annual Review of Public Health*, 29(1), 41–55. <https://doi.org/10.1146/annurev.publhealth.29.020907.090843>

- Kusaka, H., Kondo, H., Kikegawa, Y., & Kimura, F. (2001). A simple single-layer urban canopy model for atmospheric models: Comparison with multi-layer and slab models. *Boundary-Layer Meteorology*, 101(3), 329–358. <https://doi.org/10.1023/a:1019207923078>
- Li, X.-X., Koh, T.-Y., Entekhabi, D., Roth, M., Panda, J., & Norford, L. K. (2013). A multi-resolution ensemble study of a tropical urban environment and its interactions with the background regional atmosphere. *Journal of Geophysical Research: Atmospheres*, 118, 9804–9818. <https://doi.org/10.1002/jgrd.50795>
- Li, X.-X., & Norford, L. K. (2016). Evaluation of cool roof and vegetations in mitigating urban heat island in a tropical city, Singapore. *Urban Climate*, 16, 59–74. <https://doi.org/10.1016/j.uclim.2015.12.002>
- Li, Y., & Zhao, X. (2012). An empirical study of the impact of human activity on long-term temperature change in China: A perspective from energy consumption. *Journal of Geophysical Research*, 117, D17117. <https://doi.org/10.1029/2012JD018132>
- Liu, X., Tian, G., Feng, J., Wang, J., & Kong, L. (2018). Assessing summertime urban warming and the cooling efficacy of adaptation strategy in the Chengdu-Chongqing metropolitan region of China. *Science of the Total Environment*, 610–611, 1092–1102. <https://doi.org/10.1016/j.scitotenv.2017.08.082>
- Macintyre, H., & Heaviside, C. (2019). Potential benefits of cool roofs in reducing heat-related mortality during heatwaves in a European city. *Environment International*, 127, 430–441. <https://doi.org/10.1016/j.envint.2019.02.065>
- Macintyre, H., Heaviside, C., Taylor, J., Picetti, R., Symonds, P., Cai, X., & Vardoulakis, S. (2017). Assessing urban population vulnerability and environmental risks across an urban area during heatwaves—Implications for health protection. *Science of the Total Environment*, 610–611, 678–690. <https://doi.org/10.1016/j.scitotenv.2017.08.062>
- Mayocchi, C. L., & Bristow, K. L. (1995). Soil surface heat flux: Some general questions and comments on measurements. *Agricultural and Forest Meteorology*, 75(1–3), 43–50. [https://doi.org/10.1016/0168-1923\(94\)02198-S](https://doi.org/10.1016/0168-1923(94)02198-S)
- Meteorological Service Singapore (2018). Climae of Singapore. Retrieved from: <http://www.weather.gov.sg/climate-climate-of-singapore/>
- Mohajerani, A., Bakaric, J., & Jeffrey-Bailey, T. (2017). The urban heat island effect, its causes, and mitigation, with reference to the thermal properties of asphalt concrete. *Journal of Environmental Management*, 197, 522–538. <https://doi.org/10.1016/j.jenvman.2017.03.095>
- Morini, E., Touchaei, A., Castellani, B., Rossi, F., & Cotana, F. (2016). The impact of albedo increase to mitigate the urban heat island in Terni (Italy) using the WRF model. *Sustainability*, 8(10), 999. <https://doi.org/10.3390/su8100999>
- Newport Corporation (2019). Tutorial: Introduction to solar radition. Retrieved from: <https://www.newport.com/t/introduction-to-solar-radiation>
- NOAA/National Weather Service/Weather Prediction Center, The Heat Index Equation (1990). Retrieved from: https://www.wpc.ncep.noaa.gov/html/heatindex_equation.shtml
- Oak Ridge National Laboratory Distributed Active Archive Central (2016). MODIS (MCD12Q1) Land Cover (Version 005). Retrieved from https://webmap.ornl.gov/ogc/dataset.jsp?ds_id=10004
- Oke, T. R. (1982). The energetic basis of the urban heat island. *Quarterly Journal of the Royal Meteorological Society*, 108(455), 1–24. <https://doi.org/10.1002/qj.49710845502>
- Quah, A. K. L., & Roth, M. (2012). Diurnal and weekly variation of anthropogenic heat emissions in a tropical city, Singapore. *Atmospheric Environment*, 46, 92–103. <https://doi.org/10.1016/j.atmosenv.2011.10.015>
- Roth, M., & Chow, W. T. L. (2012). A historical review and assessment of urban heat island research in Singapore. *Singapore Journal of Tropical Geography*, 33(3), 381–397. <https://doi.org/10.1111/sjtg.12003>
- Satellite Imaging Corporation (2016). CARTOSAT-1 Satellite Sensor. Retrieved from <https://www.satimagingcorp.com/satellite-sensors/other-satellite-sensors/cartosat-1/>
- National Center for Atmospheric Research, USA (2008). A description of the advanced research WRF version 3. Retrieved from: <https://opensky.ucar.edu/islandora/object/technotes%3A500/datastream/PDF/view>
- Sleiman, M., Ban-Weiss, G., Gilbert, H. E., François, D., Berdahl, P., Kirchstetter, T. W., et al. (2011). Soiling of building envelope surfaces and its effect on solar reflectance—Part I: Analysis of roofing product databases. *Solar Energy Materials and Solar Cells*, 95(12), 3385–3399. <https://doi.org/10.1016/j.solmat.2011.08.002>
- Synnefa, A., Dandou, A., Santamouris, M., Tombrou, M., & Soulakellis, N. (2008). On the use of cool materials as a heat island mitigation strategy. *Journal of Applied Meteorology and Climatology*, 47(11), 2846–2856. <https://doi.org/10.1175/2008jamc1830.1>
- The Data Engineering and Curation Section of the Computational and Information Systems Laboratory at the National Center for Atmospheric Research in Boulder, Colorado (2015). NCEP GDAS/FNL 0.25 Degree Global Tropospheric Analyses and Forecast Grids. Retrieved from: <https://rda.ucar.edu/datasets/ds083.3/>
- United States Environmental Protection Agency (2008). Reducing urban heat islands: Compendium of strategies. Retrieved from: <https://www.epa.gov/heat-islands/heat-island-compendium>
- University Corporation for Atmospheric Research, Boulder, CO (2012). Overview of WRF physics. Retrieved from: http://homepages.see.leeds.ac.uk/~lecap/wiser/sample_wiser_files.dir/Physics_Dudhia.ppt.pdf
- Urban Redevelopment Authority, Singapore (2014). Master Plan 2014. Retrieved from <https://www.ura.gov.sg/Corporate/Planning/Master-Plan/Introduction>
- Yow, D. M. (2007). Urban heat islands: Observations, impacts, and adaptation. *Geography Compass*, 1(6), 1227–1251. <https://doi.org/10.1111/j.1749-8198.2007.00063.x>

References From The Supporting Information

- Collins, W. D., Rasch, P. J., Boville, B. A., Hack, J. J., McCaa, J. R., Williamson, D. L., Lin, S. (2004). Description of the NCAR community atmosphere model (CAM 3.0). *NCAR Tech. Note NCAR/TN-464+ STR*, 226.
- Dudhia, J. (1989). Numerical study of convection observed during the winter monsoon experiment using a mesoscale two-dimensional model. *Journal of the Atmospheric Sciences*, 46(20), 3077–3107. [https://doi.org/10.1175/1520-0469\(1989\)046<3077:nsocod>2.0.co;2](https://doi.org/10.1175/1520-0469(1989)046<3077:nsocod>2.0.co;2)
- Grell, G. A. (1993). Prognostic evaluation of assumptions used by cumulus parameterizations. *Monthly Weather Review*, 121(3), 764–787. [https://doi.org/10.1175/1520-0493\(1993\)121<0764:peoaub>2.0.co;2](https://doi.org/10.1175/1520-0493(1993)121<0764:peoaub>2.0.co;2)
- Grell, G. A., & Dévényi, D. (2002). A generalized approach to parameterizing convection combining ensemble and data assimilation techniques. *Geophysical Research Letters*, 29(14), 1693. <https://doi.org/10.1029/2002GL015311>
- Hong, S.-Y., Noh, Y., & Dudhia, J. (2006). A new vertical diffusion package with an explicit treatment of entrainment processes. *Monthly Weather Review*, 134(9), 2318–2341. <https://doi.org/10.1175/mwr3199.1>

- Iacono, M. J., Delamere, J. S., Mlawer, E. J., Shephard, M. W., Clough, S. A., & Collins, W. D. (2008). Radiative forcing by long-lived greenhouse gases: Calculations with the AER radiative transfer models. *Journal of Geophysical Research*, 113, D13103. <https://doi.org/10.1029/2008JD009944>
- Janjić, Z. I. (1994). The step-mountain eta coordinate model: Further developments of the convection, viscous sublayer, and turbulence closure schemes. *Monthly Weather Review*, 122(5), 927–945. [https://doi.org/10.1175/1520-0493\(1994\)122](https://doi.org/10.1175/1520-0493(1994)122)
- Kain, J. S. (2004). The Kain–Fritsch convective parameterization: An update. *Journal of Applied Meteorology*, 43(1), 170–181. [https://doi.org/10.1175/1520-0450\(2004\)043<0170:tkcpau>2.0.co;2](https://doi.org/10.1175/1520-0450(2004)043<0170:tkcpau>2.0.co;2)
- Kessler, E. (1995). On the continuity and distribution of water substance in atmospheric circulations. *Atmospheric Research*, 38(1–4), 109–145. [https://doi.org/10.1016/0169-8095\(94\)00090-Z](https://doi.org/10.1016/0169-8095(94)00090-Z)
- Liao, J., Wang, T., Wang, X., Xie, M., Jiang, Z., Huang, X., & Zhu, J. (2014). Impacts of different urban canopy schemes in WRF/Chem on regional climate and air quality in Yangtze River Delta, China. *Atmospheric Research*, 145(146), 226–243. <https://doi.org/10.1016/j.atmosres.2014.04.005>
- Mohegh, A., Rosado, P., Jin, L., Millstein, D., Levinson, R., & Ban-Weiss, G. (2017). Modeling the climate impacts of deploying solar reflective cool pavements in California cities. *Journal of Geophysical Research: Atmospheres*, 122, 6798–6817. <https://doi.org/10.1002/2017JD026845>
- Nakanishi, M., & Niino, H. (2006). An improved Mellor–Yamada Level-3 model: Its numerical stability and application to a regional prediction of advection fog. *Boundary-Layer Meteorology*, 119(2), 397–407. <https://doi.org/10.1007/s10546-005-9030-8>
- Nakanishi, M., & Niino, H. (2009). Development of an improved turbulence closure model for the atmospheric boundary layer. *Journal of the Meteorological Society of Japan. Ser. II*, 87(5), 895–912. <https://doi.org/10.2151/jmsj.87.895>
- Pleim, J. E. (2007). A combined local and nonlocal closure model for the atmospheric boundary layer. Part I: Model description and testing. *Journal of Applied Meteorology and Climatology*, 46(9), 1383–1395. <https://doi.org/10.1175/jam2539.1>
- Rogers, E., Black, T., Ferrier, B., Lin, Y., Parrish, D., & DiMego, G. (2001). Changes to the NCEP Meso Eta Analysis and Forecast System: Increase in resolution, new cloud microphysics, modified precipitation assimilation, modified 3DVAR analysis. *NWS Technical Procedures Bulletin*, 488, 15.
- Sarmiento, D. P., Davis, K. J., Deng, A., Lauvax, T., Brewer, A., & Hardesty, M. (2017). A comprehensive assessment of land surface-atmosphere interactions in a WRF/Urban modeling system for Indianapolis. *Elem Sci Anth*, 5, p.23. <http://doi.org/10.1525/elementa.132>
- Sundqvist, H., Berge, E., & Kristjánsson, J. E. (1989). Condensation and cloud parameterization studies with a mesoscale numerical weather prediction model. *Monthly Weather Review*, 117(8), 1641–1657. [https://doi.org/10.1175/1520-0493\(1989\)117<1641:CACPSW>2.0.CO;2](https://doi.org/10.1175/1520-0493(1989)117<1641:CACPSW>2.0.CO;2)
- Tao, W.-K., Simpson, J., & McCumber, M. (1989). An ice-water saturation adjustment. *Monthly Weather Review*, 117(1), 231–235. [https://doi.org/10.1175/1520-0493\(1989\)117<0231:aiwsa>2.0.co;2](https://doi.org/10.1175/1520-0493(1989)117<0231:aiwsa>2.0.co;2)
- Xu, K.-M., & Randall, D. A. (1996). A semiempirical cloudiness parameterization for use in climate models. *Journal of the Atmospheric Sciences*, 53(21), 3084–3102. [https://doi.org/10.1175/1520-0469\(1996\)053<3084:ASCPFU>2.0.CO;2](https://doi.org/10.1175/1520-0469(1996)053<3084:ASCPFU>2.0.CO;2)

Erratum

In the originally published version of this article, there was an error in the calculation of areas in Table 7. In the modeling, both the land use map and the urban fraction map are considered as inputs for setting up a land surface model. In the original version of Table 7, the calculation of areas of each cool coating surface in each urban category pixel are only based on the land use map, and the effort of fraction map was missing. Only the numbers in the table were affected. The errors have since been corrected, and this may be considered the authoritative version of record.